



## Magnetofossil spike during the Paleocene-Eocene thermal maximum: Ferromagnetic resonance, rock magnetic, and electron microscopy evidence from Ancora, New Jersey, United States

Robert E. Kopp,<sup>1,2</sup> Timothy D. Raub,<sup>3,4</sup> Dirk Schumann,<sup>5</sup> Hojatollah Vali,<sup>5</sup> Alexei V. Smirnov,<sup>3,6</sup> and Joseph L. Kirschvink<sup>1</sup>

Received 27 April 2007; revised 25 July 2007; accepted 29 August 2007; published 16 November 2007.

[1] Previous workers identified a magnetically anomalous clay layer deposited on the northern United States Atlantic Coastal Plain during the Paleocene-Eocene thermal maximum (PETM). The finding inspired the highly controversial hypothesis that a cometary impact triggered the PETM. Here we present ferromagnetic resonance (FMR), isothermal and anhysteretic remanent magnetization, first-order reversal curve, and transmission electron microscopy analyses of late Paleocene and early Eocene sediments in drill core from Ancora, New Jersey. A novel paleogeographic analysis applying a recent paleomagnetic pole from the Faeroe Islands indicates that New Jersey during the initial Eocene had a  $\sim 6^\circ$ – $9^\circ$  lower paleolatitude ( $\sim 27.3^\circ$  for Ancora) and a more zonal shoreline trace than in conventional reconstructions. Our investigations of the PETM clay from Ancora reveal abundant magnetite nanoparticles bearing signature traits of crystals produced by magnetotactic bacteria. This result, the first identification of ancient biogenic magnetite using FMR, argues that the anomalous magnetic properties of the PETM sediments are not produced by an impact. They instead reflect environmental changes along the eastern margin of North America during the PETM that led to enhanced production and/or preservation of magnetofossils.

**Citation:** Kopp, R. E., T. D. Raub, D. Schumann, H. Vali, A. V. Smirnov, and J. L. Kirschvink (2007), Magnetofossil spike during the Paleocene-Eocene thermal maximum: Ferromagnetic resonance, rock magnetic, and electron microscopy evidence from Ancora, New Jersey, United States, *Paleoceanography*, 22, PA4103, doi:10.1029/2007PA001473.

### 1. Introduction

[2] The Paleocene-Eocene boundary is followed by a  $\sim 5^\circ$ – $9^\circ\text{C}$  global warming event, the Paleocene-Eocene thermal maximum (PETM, also known as the initial Eocene thermal maximum (IETM)) [Bowen *et al.*, 2006]. The PETM begins with the rapid onset of a  $-3$  to  $-5\%$  carbon isotope excursion in carbonate, which suggests that the warming was linked to increased atmospheric greenhouse gas concentrations. The climatic event led to changes in the hydrologic cycle, which in turn altered the character of sediments deposited throughout the world. In many continental margin sections, the PETM is associated with thick, siliclastic deposits, presumably reflecting enhanced fluvial sediment delivery [e.g., Crouch *et al.*, 2003; Gawenda *et*

*al.*, 1999; Giusberti *et al.*, 2007; Schmitz and Pujalte, 2003]. In the Atlantic Coastal Plain of the northeastern United States, PETM sections are expanded, depleted in sand-sized particles and enriched in clay-sized kaolinite [Gibson *et al.*, 1993, 2000; Kent *et al.*, 2003]. Kent *et al.* [2003] found that PETM sediments from New Jersey also had anomalous magnetic properties indicating enrichment of fine-grained, single-domain (SD) magnetite.

[3] Kent *et al.* [2003] considered two hypotheses for the origin of the SD magnetite: production by magnetotactic bacteria and production as a fallout condensate following a cometary impact. Magnetotactic bacteria synthesize intracellular chains of SD, frequently elongate crystals of magnetite or greigite, which can be preserved in sediments as magnetofossils. Common in both freshwater and marine environments, the bacteria are most abundant under suboxic conditions, both in sediments and in the water column. Although magnetofossils are common magnetic components of Quaternary sediments [Petersen *et al.*, 1986], reports of magnetofossils from older rocks are scarce [Evans and Heller, 2003; Kopp and Kirschvink, 2007]. Kent *et al.* dismissed the possibility that the magnetic properties of the New Jersey PETM clay were produced by magnetofossils because they imaged only isolated, equidimensional magnetite under transmission electron microscopy (TEM). The production of a similarly anomalous magnetic nanophase, albeit one composed of ferric oxyhydroxides, as fallout condensate from the end-Cretaceous impact [Wdowiak *et*

<sup>1</sup>Division of Geological and Planetary Sciences, California Institute of Technology, Pasadena, California, USA.

<sup>2</sup>Now at Department of Geosciences, Princeton University, Princeton, New Jersey, USA.

<sup>3</sup>Department of Geology and Geophysics, Yale University, New Haven, Connecticut, USA.

<sup>4</sup>Now at Division of Geological and Planetary Sciences, California Institute of Technology, Pasadena, California, USA.

<sup>5</sup>Department of Earth and Planetary Sciences, McGill University, Montreal, Quebec, Canada.

<sup>6</sup>Now at Department of Geological and Mining Engineering and Sciences, Michigan Technological University, Houghton, Michigan, USA.

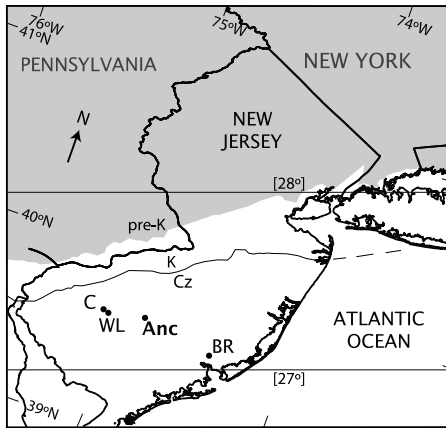


**Figure 1.** Paleogeographic map of New Jersey drill sites. From west to east, sites are Clayton (C), Wilson Lake (WL), Ancora (Anc), and Bass River (BR). Cenozoic (Cz), Cretaceous (K), and pre-Cretaceous (pre-K) outcrop limits are shown [Van Sickle *et al.*, 2004]. Paleolatitude, shown in brackets, is derived from the Faeroe Islands paleopole of Riisager *et al.* [2002] rotated using the Rockall microplate parameters of Royer *et al.* [1991].

*al.*, 2001] led them to hypothesize instead that the PETM was a “bolide summer” triggered by a cometary impact [Cramer and Kent, 2005; Kent *et al.*, 2003].

[4] Aside from the magnetic anomaly, which has no known analog that persists in the rock record for a duration comparable to that of the PETM, Kent *et al.* [2003] marshaled two other arguments in support of their controversial proposal: the presence of a small iridium anomaly at the beginning of the PETM in a section at Zumaya, Spain, and the ability of the bolide hypothesis to explain the geologically instantaneous injection of isotopically light carbon into the ocean-atmospheric system. They also suggested that the deposition of kaolinite-rich sediments might be linked to redeposition of impact ejecta. They acknowledged some evidence against their model, specifically: (1) the absence of an impact crater, which they attributed to a marine impact, (2) the absence of an observed depletion in  $^{187}\text{Os}/^{188}\text{Os}$  ratios, characteristic of extraterrestrial material, which they attributed to undersampling, and (3) the absence of a peak in extraterrestrial helium, which is carried by fine-grained interplanetary dust particles rather than large impactors and is also not observed at the end-Cretaceous [Mukhopadhyay *et al.*, 2001]. Schmitz *et al.* [2004] examined platinum group elements (PGEs) in six marine PETM sections from Egypt, Spain, and Denmark. Only the Zumaya section exhibited a small Ir enrichment, and the PGE ratios of the enriched bed were inconsistent with a significant extraterrestrial component. Os isotopes also did not provide evidence for an extraterrestrial component. Dickens and Francis [2004] argued that the results of Kent *et al.* were better explained by pore water redox changes along the New Jersey continental margin that resulted in an enrichment of biogenic magnetite.

[5] As a test of the bolide impact and magnetofossil hypotheses, we present in this paper new ferromagnetic resonance (FMR), isothermal and anhysteretic remanent magnetization (IRM and ARM), first-reversal curve (FORC), and transmission electron microscopy (TEM) analyses of PETM shelf sediments from one of the drill cores Kent *et al.* studied, Ancora. Elsewhere in this issue, Lippert and Zachos [2007] present an independent rock magnetic and TEM study of correlative sediments from the more shoreward Wilson Lake drill core. Recent rock magnetic analyses of continental margin sediments from Marlborough, South Island, New Zealand, suggest that the distinctive magnetic properties observed in New Jersey are not a global phenomenon [Villasante-Marcos *et al.*, 2007].

## 2. Geological Setting

[6] Ocean Drilling Program Leg 174AX recovered cores from two continental sections containing late Paleocene and early Eocene shallow marine deposits, at Bass River and Ancora, New Jersey [Miller *et al.*, 1998] (Figure 1). Paleocene-Eocene sediments from Bass River were deposited at  $\sim 105\text{--}140$  m water depth, while sediments from Ancora were deposited at  $\sim 45\text{--}70$  m water depth [Van Sickle *et al.*, 2004]. The United States Geological Survey drilled a core through shallower water depth sediments at Clayton, New Jersey [Gibson *et al.*, 1993], later supplemented with another at nearby Wilson Lake,  $\sim 5$  km east of Clayton [Zachos *et al.*, 2006].

[7] The four sites record a  $\sim 5\%$  carbon isotopic excursion (CIE) in bulk carbonate, associated with the PETM, in  $\sim 5$  to  $\sim 20$  m of kaolinite-rich clay with low quartz content. The clay layer interrupts otherwise quartzose and glauconitic silt and sand. In the Ancora drill core, a marked decrease in carbon isotopic composition occurs between 172.5 and 171.3 m, while the shift from quartzose and glauconitic sand and silt to kaolinitic clay occurs between 171.9 and 170.7 m. A partial carbon isotopic recovery occurs between 166.3 and 165.2 m, while the sediments become more sand rich at 165.2 m and above (Figure 2).

[8] Kent *et al.* [2003] found that the PETM clay exhibits high ratios of saturation-remanent magnetization ( $M_r$ ) to saturation magnetization ( $M_s$ ) that reach values exceptional for sedimentary rocks and close to the theoretical uniaxial, SD magnetite limit of 0.50. The highest ratios are exhibited in the shallower cores:  $M_r/M_s$  during the PETM is nearly uniformly  $\sim 0.40$  at Clayton and  $\sim 0.35$  at Ancora (Figure 2), while at more distal Bass River,  $M_r/M_s$  varies within the belt between  $\sim 0.10$  and  $\sim 0.30$  [Kent *et al.*, 2003]. Lippert and Zachos [2007] profile magnetic hysteresis parameters through the Wilson Lake drill core, proximal to Clayton.

[9]  $M_s$  values indicate that the PETM sediments with high  $M_r/M_s$  contain  $\sim 120\text{--}200$  ppm of predominantly SD magnetite, whereas underlying and overlying sediments contain  $\sim 30\text{--}70$  ppm predominantly detrital, mostly multidomain magnetite. Magnetic and carbon isotopic data from the Ancora core record the onset of the magnetic anomaly over the  $\sim 40$  cm above the onset of CIE (Figure 2 and Table S1

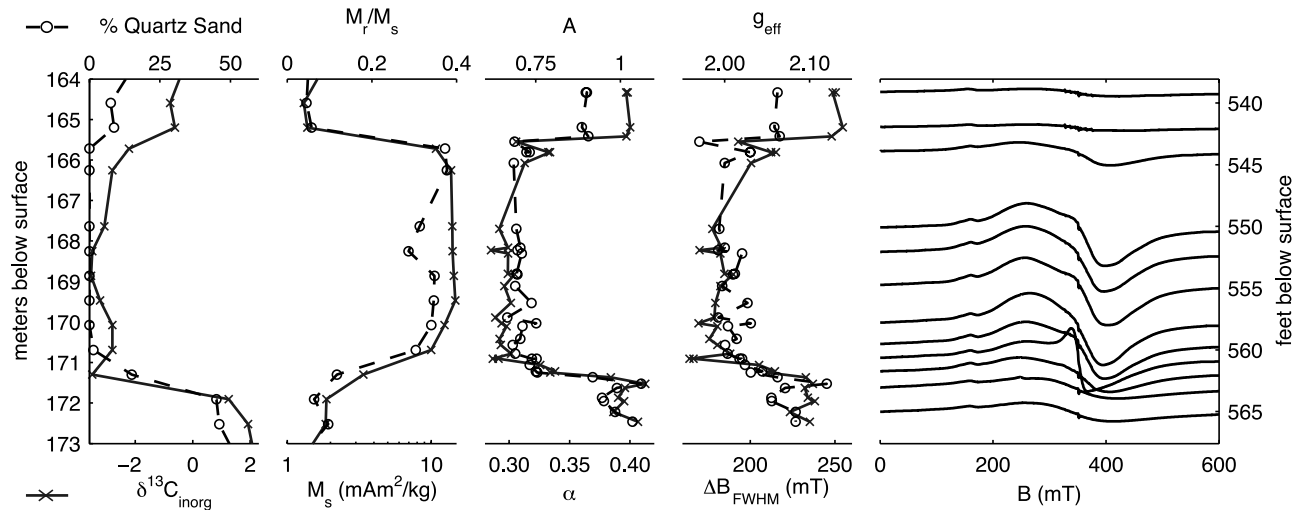


**Figure 2.** Fine quartz sand fraction,  $\delta^{13}\text{C}_{\text{inorganic}}$ , ratio of saturation remanence magnetization to saturation magnetization, saturation magnetization (all from *Kent et al.* [2003]), FMR parameters  $\alpha$ ,  $A$ ,  $\Delta B_{\text{FWHM}}$ , and  $g_{\text{eff}}$  and example FMR spectra for upper Paleocene to lower Eocene strata, Ocean Drilling Program Leg 174AX, Ancora, New Jersey. Left edges of example spectra align with drill core depth.

of the auxiliary material<sup>1</sup>, between 171.3 and 170.9 m) [*Kent et al.*, 2003]. Assuming constant clay sedimentation rate during the PETM, this lag of  $\sim 8\%$  of the event's total  $\sim 100\text{--}200$  ka duration [*Farley and Eltgroth*, 2003; *Rohl et al.*, 2000] represents  $\sim 9\text{--}18$  ka. Since kaolinite fraction decreases upward through the PETM clay at Clayton while magnetic parameters remain effectively constant, and since Bass River preserves magnetic variation throughout the lithologically homogeneous clay interval, the anomalous magnetic properties do not appear to be produced by lithological changes.

### 3. Paleogeographic Setting

[10] A relatively new, high-quality paleomagnetic pole from Faeroe Islands flood volcanics [*Riisager et al.*, 2002], effectively coincident with the  $\sim 55.6$  Ma PETM [*Storey et al.*, 2007], yields a paleolatitude of  $\sim 27.3^\circ$  at Ancora, New Jersey. This paleolatitude is well within the modern and ancient evaporite belt ( $\sim 15^\circ\text{--}35^\circ$ ) [*Evans*, 2006] and consistent with suggestions of a regional land surface devoid of terrestrial vegetation [*Zachos et al.*, 2006]. Assuming the reconstructed traces of Appalachian basement and Cretaceous cover outcrop belts are parallel with the ancient shoreline, the facing direction  $\sim 19.6^\circ$  west of modern north indicates a nearly east-west shoreline trace (Figure 1).

[11] To our knowledge, this Faeroe Islands pole has not previously been applied to the PETM, though *Riisager et al.* [2002] argue that it should supersede prior North Atlantic Igneous Province results, upon which most Paleocene-Eocene paleogeographies are based. The resulting paleolatitude is  $\sim 6^\circ\text{--}9^\circ$  lower than in conventional reconstructions

(auxiliary material Table S3), and the derived shoreline trace is more zonal. We calculate Ancora paleolatitudes using conventional paleopoles and comment on the reconstruction procedure in the auxiliary material.

## 4. Methods

### 4.1. Sampling

[12] The Ancora drill core (IODP Leg 174AX) is stored at the Rutgers/New Jersey Geological Survey Rift-Drift Core Repository. Thirty-one samples were collected between 164.33 m (539.14 feet) and 172.46 m (565.83 feet), an interval that includes the PETM.

### 4.2. Ferromagnetic Resonance

[13] FMR measurements were made using an X band Bruker ESP 300E EPR spectrometer [*Kopp et al.*, 2006]. About 200–1000 mg of each freeze-dried sediment sample were loaded into quartz glass EPR tubes. Since the sediment filled the sample cavity, measurements of total absorption were effectively volume normalized. The spectra were measured at  $640 \mu\text{W}$  of microwave power and summed over three magnetic sweeps from 0 to 600 mT.

[14] We quantify FMR spectra using four empirical parameters:  $g_{\text{eff}}$ ,  $A$ ,  $\Delta B_{\text{FWHM}}$ , and  $\alpha$  [*Kopp et al.*, 2006]. The effective g factor  $g_{\text{eff}}$  is the g factor at which peak absorption occurs. The asymmetry ratio  $A$  is  $\Delta B_{\text{low}}/\Delta B_{\text{high}}$ , where the half widths at half maximum,  $\Delta B_{\text{low}}$  and  $\Delta B_{\text{high}}$ , are the distance from the absorption maximum to the low-field and half-field half maximum, respectively. Spectra extended in the low-field direction have  $A < 1$ , which reflects the anisotropy produced by uniaxial elongation or linear particle arrangements. Isolated, equidimensional particles have  $A \sim 1$ . The full width at half maximum  $\Delta B_{\text{FWHM}}$  is  $\Delta B_{\text{low}} + \Delta B_{\text{high}}$ . The empirical discriminant factor  $\alpha$  (defined as  $0.17 A + 9.8 \times 10^{-4} \Delta B_{\text{FWHM}}/\text{mT}$ )

<sup>1</sup>Auxiliary materials are available in the HTML. doi:10.1029/2007PA001473.

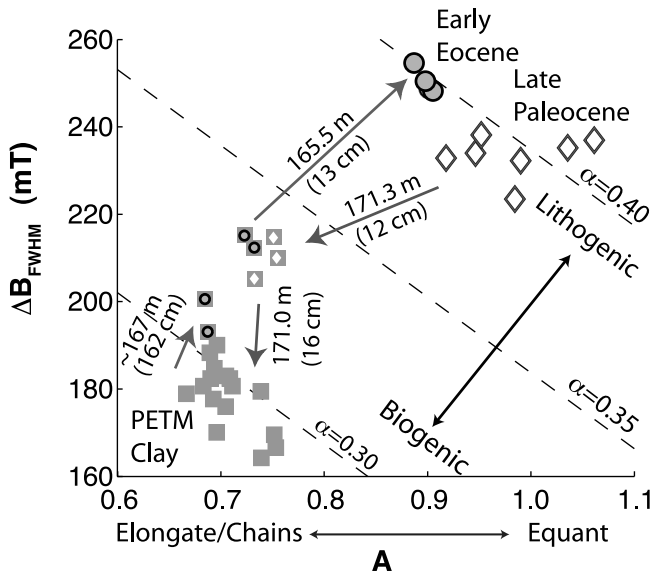


**Figure 3.** FMR parameters  $\Delta B_{FWHM}$  and  $A$  for PETM clay (grey squares, lowermost clay shown by grey squares with white diamonds, uppermost clay shown by grey squares with black circles) and underlying (open diamonds) and overlying (grey circles) sediments. Arrows, showing transitions between populations, are labeled with transition depth and unsampled interval thickness. Detrital-dominated sediments generally have  $\alpha > 0.40$ , while previously studied pelagic magnetofossil-rich sediments have  $\alpha < 0.30$  [Kopp et al., 2006].

reflects the homogeneity of magnetic particles. Particles with narrow size and shape distributions, such as magnetofossils, have asymmetric but relatively narrow spectra and therefore have low  $\alpha$  (typically,  $\alpha < 0.25$  for bacterial cultures and  $\alpha < \sim 0.3$  for magnetofossils), while particles with broad distributions, such as detrital particles, have high  $\alpha$  (typically  $\alpha > \sim 0.4$ ).

#### 4.3. Transmission Electron Microscopy

[15] Magnetic separates were extracted from clay mineral samples dispersed in distilled water using a magnetic finger [Petersen et al., 1986], transferred onto C-coated 300-mesh Cu TEM grids and studied using a JEOL JEM-2000FX TEM and a JEOL-JEM 2100F FE-TEM, the latter equipped with an Oxford INCA microanalytical system. High-resolution lattice-fringe images and diffraction patterns were obtained at 200 kV accelerating voltage.

#### 4.4. Rock Magnetism

[16] IRM, ARM, and FORC procedures and results are detailed in the auxiliary material.

### 5. Characterization of Magnetic Particles

[17] FMR spectroscopy is an electron spin resonance technique capable of assessing the magnetic anisotropy, magnetic interactions, and morphological heterogeneity of magnetic particles in bulk samples [Kopp et al., 2006]. It is thus ideally suited for distinguishing among (1) detrital

magnetite, (2) isolated particles of equidimensional magnetite, and (3) magnetofossils, which are frequently elongate and often preserved in chains. FMR can therefore readily check the observation that magnetite in the PETM sediments occurs as isolated, equidimensional particles, the finding that spurred the “bolide summer” hypothesis [Kent et al., 2003]. FMR parameters of latest Paleocene to early Eocene sediments from the Ancora drill core confirm that pre-CIE and post-CIE siltstones are dominated by presumably detrital magnetic particles with broad size distributions and indicate that the PETM clay hosts fairly homogeneous magnetic populations of elongate particles and/or chains, consistent with magnetofossils rather than isolated, equidimensional particles (Figures 2 and 3 and auxiliary Table S1). A sand lens within the upper portion of the clay (at 165.81 m) has nearly identical FMR properties to the surrounding clay, which supports the hypothesis that grain size is not controlling the change in magnetic properties.

[18] TEM and energy dispersive X-ray spectroscopy analysis of magnetic separates [Petersen et al., 1986] from suspended clay reveals abundant elongate prismatic and bullet-shaped, SD-size crystals of stoichiometric magnetite (Figures 4 and 5) that resemble magnetite present within a variety of bacteria [Kopp and Kirschvink, 2007; Vali and Kirschvink, 1991]. Equidimensional cuboidal particles are present but less common than elongate particles. Although equidimensional magnetite particles can have many origins, the particles in the clay have a tight size and shape distribution almost entirely within the SD field (Figure 5), consistent with a bacterial source. Some particles show irregular shapes that suggest minor dissolution. The bullet-shaped particles reach sizes that, to our knowledge, exceed the size of previously reported magnetofossils but are consistent with the largest bullet-shaped particles observed in living bacteria [Vali and Kirschvink, 1991].

[19] In the separates, particles with similar morphologies occasionally form short chains of 3–5 crystals, possibly remnants of biologically generated chain structures. FMR data, as well as rock magnetic data from first-order reversal curve (FORC) analyses and remanent magnetization experiments (see auxiliary material), indicate that most of the magnetic material exists in situ either as isolated particles or as chains, some of which may have been disrupted during the magnetic separation process. However, FMR and FORC analysis also indicate limited but nonnegligible particle interaction fields, which suggests some in situ aggregation of particles in clumps. Consistent with FMR and rock magnetic data, magnetic separates from silts and sands deposited before and after the CIE did not include any putative magnetofossils.

### 6. Environmental Implications

[20] Similar, though shorter duration and less pronounced, climate-linked increases in magnetofossil abundance have been observed in Quaternary pelagic and hemipelagic sediments [Dinarès-Turell et al., 2003; Hesse, 1994; Lean and McCave, 1998]. In these sediments, magnetofossil abundance is generally lower in glacial periods and higher in interglacial deposits. Observations of the degree of biotur-

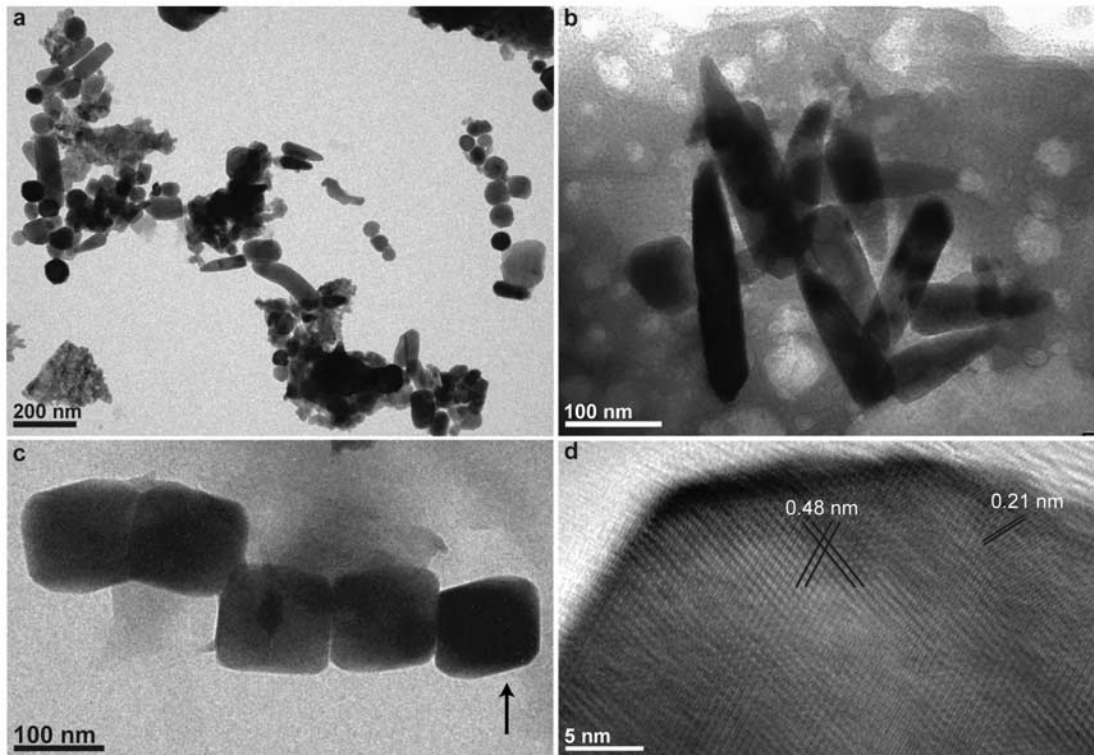


**Figure 4.** TEM images of magnetic particles separated from Ancora samples: (a) an assemblage of cuboidal, prismatic, and bullet-shaped particles resembling bacterial magnetite, (b) bullet-shaped magnetite particles, (c) a chain-like arrangement of prismatic particles, and (d) a high-resolution image of a single crystal (arrow in Figure 4c). Figure 4b is from 168.81 m depth; Figures 4a, 4c, and 4d are from 170.41 m depth. Variation in contrast of the individual particles is due to the crystal orientation with respect to the electron beam. Figure 4d shows two sets of intersecting  $\{111\}$  and  $\{200\}$  lattice fringes with a spacing of 0.48 nm and 0.21 nm, respectively. The measured intersection angle between the  $\{111\}$  set is  $71^\circ$ .

bation, sediment color, and organic carbon content suggest that increased pore water oxygen during interglacial stages drives the change. Increased pore water oxygen, which at a constant sedimentation rate could result from a reduced flux of organic carbon to sediments or enhanced bottom water oxygen content [van der Loeff, 1990], will increase the depth at which anoxia occurs within the sediments. The suboxic zone of the sediments, in which most magnetotactic bacteria live, will expand and likely cause the total population of magnetotactic bacteria to grow. Moreover, because fine-grained magnetite dissolves readily under fully anoxic conditions, an expanded suboxic zone will foster better magnetofossil preservation, a taphonomic bias that exaggerates the ecological effect.

[21] We therefore suggest that the initial Eocene enrichment of magnetofossils in shallow water New Jersey sediments is linked to expanded sedimentary suboxia. Factors potentially contributing to the biogeochemical change include changes in sedimentation rate, biological productivity, oxygen solubility, and ocean circulation. By diluting sedimentary organic carbon, an increase in the ratio of sedimentation rate to productivity would increase the depth and thickness of the suboxic zone, as previously suggested by

*Dickens and Francis* [2004]. A decrease in oxygen solubility would allow suboxic and anoxic conditions to develop at shallower depths. Changes in ocean circulation could directly alter bottom water oxygen levels, as well as influencing biological productivity and, via ocean temperature, oxygen solubility.

[22] The PETM sedimentation rate on the Atlantic Coastal Plain,  $\sim 20\text{--}50$  m/My, was significantly higher than the late Paleocene and early Eocene background sedimentation rate in Ancora, estimated at  $\sim 5\text{--}10$  m/My [Van Sickel *et al.*, 2004]. If biological productivity and organic carbon preservation were constant, the  $\sim 4\text{--}5$  fold increase in sedimentation rate should produce a comparable decrease in organic carbon content. At Wilson Lake, however, organic carbon content predominantly remains  $\sim 0.3\%$  to  $\sim 0.4\%$  before, during, and after the CIE [Lippert and Zachos, 2007; Zachos *et al.*, 2006]. Moreover, because particles with high mineral surface area generally preserve organic carbon better than coarser particles [Hedges and Keil, 1995], clay sediments deposited during the CIE should more effectively preserve organic carbon than the underlying and overlying silts. The absence of the expected increase in carbon content likely reflects dilution caused by an

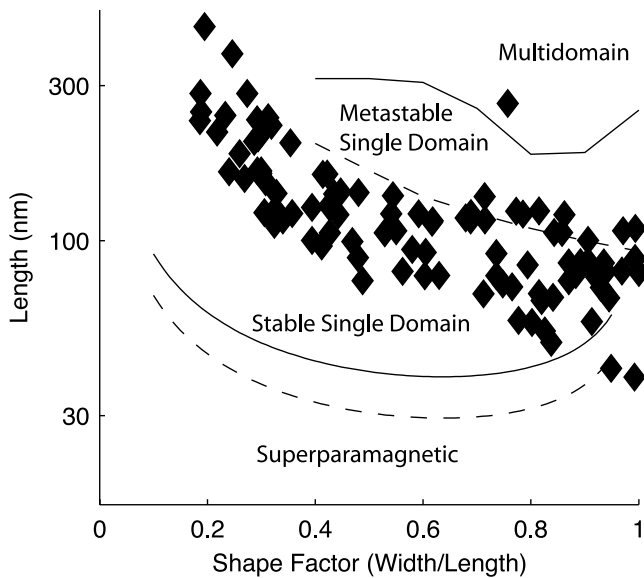


**Figure 5.** Length and shape factor (width/length ratio) of magnetite particles from 168.81 m depth. The lower, SD/superparamagnetic boundary is determined for rectangular parallelepipeds with unblocking times of 100 s (bottom dashed line) and 4.5 Ga (bottom solid line) [Butler and Banerjee, 1975; Diaz-Ricci and Kirschvink, 1992]. The top solid line and top dashed line show the upper boundary of the metastable single-domain field and stable single-domain field, respectively [Witt et al., 2005].

increased ratio of sedimentation rate to biological production. Although nanofossil assemblages at Wilson Lake during the PETM indicate a shift from oligotrophic to mesotrophic nanoplankton taxa [Gibbs et al., 2006] and are generally interpreted as reflecting increased nutrient input and productivity, both the abundance of magnetofossils and the consistently low organic carbon content preclude a productivity enhancement large enough to drive bottom water anoxia.

[23] Temperature increase during the PETM also could have contributed to the magnetofossil enrichment. Measurements of crenarcheotal lipids from Wilson Lake indicate that the sea surface temperature of the Atlantic Coastal Plain warmed from  $\sim 25^{\circ}\text{C}$  to  $\sim 33^{\circ}\text{C}$  [Zachos et al., 2006]. The

warming would have decreased oxygen solubility by  $\sim 12\%$  ( $\sim 25\ \mu\text{M}$ ) [Drever, 1997], facilitating the development of suboxic conditions.

## 7. Conclusions

[24] Kent et al. [2003] examined kaolinite-rich clay sediments deposited during the Paleocene-Eocene thermal maximum (PETM) along the northern U.S. Atlantic Coastal Margin and found that they were magnetically unusual, the thickest sections dominated by single domain magnetite yet recognized in the stratigraphic record. We reanalyzed sediments from one of their drill cores, from Ancora, New Jersey, using ferromagnetic resonance (FMR) spectroscopy, a technique recently adapted for the identification of fossil magnetotactic bacteria [Kopp et al., 2006]. The results, confirmed by electron microscopy, indicate that the magnetic properties of the clay are produced by magnetofossils, not the impact fallout condensate proposed by Kent et al. This finding is the first identification of magnetofossils in ancient sediments by FMR and validates the use of the technique for this purpose.

[25] A paleogeographic reinterpretation, based upon a new pole from the Faeroe Islands [Riisager et al., 2002], indicates that the magnetofossil-rich sediments were deposited at subtropical latitudes along a southward facing portion of the eastern margin of North America. On the basis of work linking magnetofossil populations and Quaternary climate change, we suggest that the unusual magnetic character of the sediments is the result of enhanced sedimentary suboxia during the PETM, driven by some combination of increased sediment accumulation rate, changes in biological productivity, higher temperatures, and changes in ocean circulation along the continental margin. These changes enhanced the growth of magnetotactic bacteria and/or the preservation of their fossils during the period of extreme global warmth.

[26] **Acknowledgments.** We thank A. Maloof, D. Evans, M. Pagani, E. Thomas, and K. Turekian for comments on an earlier version of this article and G. Dickens for spurring R.E.K.'s initial interest in magnetically anomalous PETM sediments. We thank D. Kent and the Ocean Drilling Program for access to samples and also thank D. Kent for access to the Rutgers AGM. NASA and the Agouron Institute provided support through grants to J.L.K. The Natural Sciences and Engineering Research Council of Canada provided support through a grant to H.V.

## References

- Bowen, G. J., et al. (2006), Eocene hyperthermal event offers insight into greenhouse warming, *Eos Trans. AGU*, 87, 165.
- Butler, R. F., and S. K. Banerjee (1975), Theoretical single-domain grain size range in magnetite and titanomagnetite, *J. Geophys. Res.*, 80, 4049–4058.
- Cramer, B. S., and D. V. Kent (2005), Bolide summer: The Paleocene/Eocene thermal maximum as a response to an extraterrestrial trigger, *Palaeogeogr. Palaeoclimatol. Palaeoecol.*, 224, 144–166.
- Crouch, E. M., G. R. Dickens, H. Brinkhuis, M.-P. Aubry, C. J. Hollis, K. M. Rogers, and H. Visscher (2003), The Apectodinium acme and terrestrial discharge during the Paleocene-Eocene thermal maximum: New palynological, geochemical and calcareous nanoplankton observations at Tawanui, New Zealand, *Palaeogeogr. Palaeoclimatol. Palaeoecol.*, 194, 387–403.
- Diaz-Ricci, J. C., and J. L. Kirschvink (1992), Magnetic domain state and coercivity predictions for biogenic greigite ( $\text{Fe}_3\text{S}_4$ ): A comparison of theory with magnetosome observations, *J. Geophys. Res.*, 97, 17,309–17,315.
- Dickens, G. R., and J. M. Francis (2004), Comment on “A case for a comet impact trigger for the Paleocene/Eocene thermal maximum and carbon isotope excursion” by D. V. Kent et al. [*Earth Planet. Sci. Lett.* 211(2003) 13–26], *Earth Planet. Sci. Lett.*, 217, 197–200.
- Dinarès-Turell, J., B. A. A. Hoogakker, A. P. Roberts, E. J. Rohling, and L. Sagnotti (2003), Quaternary climatic control of biogenic magnetite production and eolian dust input in cores from the Mediterranean Sea, *Palaeogeogr. Palaeoclimatol. Palaeoecol.*, 190, 195–209.
- Drever, J. L. (1997), *The Geochemistry of Natural Waters*, 3rd ed., 436 pp., Prentice Hall, Upper Saddle River, N. J.
- Evans, D. A. D. (2006), Proterozoic low orbital obliquity and axial-dipolar geomagnetic field from evaporite palaeolatitudes, *Nature*, 442, 51–55.

- Evans, M. E., and F. Heller (2003), *Environmental Magnetism*, 299 pp., Academic, San Diego, Calif.
- Farley, K. A., and S. F. Eltgroth (2003), An alternative age model for the Paleocene-Eocene thermal maximum using extraterrestrial  $^3\text{He}$ , *Earth Planet. Sci. Lett.*, **208**, 135–148.
- Gawenda, P., W. Winkler, B. Schmitz, and T. Adatte (1999), Climate and bioproductivity control on carbonate turbidite sedimentation (Paleocene to earliest Eocene, Gulf of Biscay, Zumaia, Spain), *J. Sediment. Res.*, **69**, 1253–1261.
- Gibbs, S. J., T. J. Bralower, P. R. Bown, J. C. Zachos, and L. M. Bybell (2006), Shelf and open-ocean calcareous phytoplankton assemblages across the Paleocene-Eocene thermal maximum: Implications for global productivity gradients, *Geology*, **34**, 233–236.
- Gibson, T. G., L. M. Bybell, and J. P. Owens (1993), Latest Paleocene lithologic and biotic events in neritic deposits of southwestern New Jersey, *Paleoceanography*, **8**, 495–514.
- Gibson, T. G., L. M. Bybell, and D. B. Mason (2000), Stratigraphic and climatic implications of clay mineral changes around the Paleocene/Eocene boundary of the northeastern US margin, *Sediment. Geol.*, **134**, 65–92.
- Giusberti, L., D. Rio, C. Agnini, J. Backman, E. Fornaciari, F. Tateo, and M. Oddone (2007), Mode and tempo of the Paleocene-Eocene thermal maximum in an expanded section from the Venetian pre-Alps, *Geol. Soc. Am. Bull.*, **119**, 391–412.
- Hedges, J. I., and R. G. Keil (1995), Sedimentary organic matter preservation: An assessment and speculative synthesis, *Mar. Chem.*, **49**, 81–115.
- Hesse, P. P. (1994), Evidence for bacterial paleoecological origin of mineral magnetic cycles in oxic and sub-oxic Tasman Sea sediments, *Mar. Geol.*, **117**, 1–17.
- Kent, D. V., B. S. Cramer, L. Lanci, D. Wang, J. D. Wright, and R. Van der Voo (2003), A case for a comet impact trigger for the Paleocene/Eocene thermal maximum and carbon isotope excursion, *Earth Planet. Sci. Lett.*, **211**, 13–26.
- Kopp, R. E., and J. L. Kirschvink (2007), The identification and biogeochemical interpretation of fossil magnetotactic bacteria, *Earth Sci. Rev.*, doi:10.1016/j.earscirev.2007.08.001, in press.
- Kopp, R. E., B. P. Weiss, A. C. Maloof, H. Vali, C. Z. Nash, and J. L. Kirschvink (2006), Chains, clumps, and strings: Magnetofossil taphonomy with ferromagnetic resonance spectroscopy, *Earth Planet. Sci. Lett.*, **247**, 10–25.
- Lean, C. M. B., and I. N. McCave (1998), Glacial to interglacial mineral magnetic and paleoceanographic changes at Chatham Rise, SW Pacific Ocean, *Earth Planet. Sci. Lett.*, **163**, 247–260.
- Lippert, P. C., and J. C. Zachos (2007), A biogenic origin for anomalous fine-grained magnetic material at the Paleocene-Eocene boundary at Wilson Lake, New Jersey, *Paleoceanography*, doi:10.1029/2007PA001471, in press.
- Miller, K. G., et al. (1998) *Proceedings of the Ocean Drilling Program, Initial Reports*, vol.174, Ocean Drill. Program, College Station, Tex.
- Mukhopadhyay, S., K. A. Farley, and A. Montanari (2001), A short duration of the Cretaceous-Tertiary boundary event: Evidence from extraterrestrial helium-3, *Science*, **291**, 1952–1955.
- Petersen, N., T. von Dobeneck, and H. Vali (1986), Fossil bacterial magnetite in deep-sea sediments from the South Atlantic Ocean, *Nature*, **320**, 611–615.
- Riisager, P., J. Riisager, N. Abrahamsen, and R. Waagstein (2002), New paleomagnetic pole and magnetostratigraphy of Faroe Islands flood volcanics, North Atlantic igneous province, *Earth Planet. Sci. Lett.*, **201**, 261–276.
- Rohl, U., T. J. Bralower, R. D. Norris, and G. Wefer (2000), New chronology for the late Paleocene thermal maximum and its environmental implications, *Geology*, **28**, 927–930.
- Royer, J.-Y., R. D. Müller, L. M. Gahagan, L. A. Lawyer, C. L. Mayes, D. Nürnberg, and J. G. Sclater (1991), A global isochron chart, *Tech. Rep. 117*, 38 pp., Univ. of Texas Inst. for Geophys., Austin.
- Schmitz, B., and V. Pujalte (2003), Sea-level, humidity, and land-erosion records across the initial Eocene thermal maximum from a continental-marine transect in northern Spain, *Geology*, **31**, 689–692.
- Schmitz, B., B. Peucker-Ehrenbrink, C. Heilmann-Clausen, G. Aberg, F. Asaro, and C.-T. A. Lee (2004), Basaltic explosive volcanism, but no comet impact, at the Paleocene–Eocene boundary: High-resolution chemical and isotopic records from Egypt, Spain and Denmark, *Earth Planet. Sci. Lett.*, **225**, 1–17.
- Storey, M., R. A. Duncan, and C. C. Swisher III (2007), Paleocene-Eocene thermal maximum and the opening of the northeast Atlantic, *Science*, **316**, 587–589.
- Vali, H., and J. L. Kirschvink (1991), Observations of magnetosome organization, surface structure, and iron biomineralization of undescribed magnetic bacteria: Evolutionary speculations, in *Iron Biominerals*, edited by R. B. Frankel and R. P. Blakemore, pp. 97–116, Plenum, New York.
- van der Loeff, M. M. R. (1990), Oxygen in pore waters of deep-sea sediments, *Philos. Trans. R. Soc. London, Ser. A*, **331**, 69–84.
- Van Sickle, W. A., M. A. Kominz, K. G. Miller, and J. V. Browning (2004), Late Cretaceous and Cenozoic sea-level estimates: Backstripping analysis of borehole data, onshore New Jersey, *Basin Res.*, **16**, 451–465.
- Villasante-Marcos, V., C. J. Hollis, G. R. Dickens, and M. J. Nicolo (2007), Rock magnetic properties across the Paleocene-Eocene thermal maximum in Marlborough, New Zealand, *Geol. Acta*, in press.
- Wdowiak, T. J., L. P. Armendarez, D. G. Agresti, M. L. Wade, S. Y. Wdowiak, P. Claeys, and G. Izett (2001), Presence of an iron-rich nanophase material in the upper layer of the Cretaceous-Tertiary boundary clay, *Meteorit. Planet. Sci.*, **36**, 123–133.
- Witt, A., K. Fabian, and U. Bleil (2005), Three-dimensional micromagnetic calculations for naturally shaped magnetite: Octahedra and magnetosomes, *Earth Planet. Sci. Lett.*, **233**, 311–324.
- Zachos, J. C., S. Schouten, S. Bohaty, T. Quattlebaum, A. Sluijs, H. Brinkhuis, S. J. Gibbs, and T. J. Bralower (2006), Extreme warming of mid-latitude coastal ocean during the Paleocene-Eocene thermal maximum: Inferences from TEX86 and isotope data, *Geology*, **34**, 737–740.

J. L. Kirschvink and T. D. Raub, Division of Geological and Planetary Sciences, California Institute of Technology, Pasadena, CA 91125, USA.

R. E. Kopp, Department of Geosciences, Princeton University, Princeton, NJ 08544, USA. (rkopp@princeton.edu)

D. Schumann and H. Vali, Department of Earth and Planetary Sciences, McGill University, Montreal, Que., Canada H3A 2A7.

A. V. Smirnov, Department of Geological and Mining Engineering and Sciences, Michigan Technological University, Houghton, MI 49931, USA.

Auxiliary Material Submission for Paper  
2007PA001473

Magnetofossil spike during the Paleocene-Eocene Thermal Maximum  
Robert E. Kopp (California Institute of Technology),  
Timothy D. Raub (Yale University),  
Dirk Schumann (McGill University),  
Hojatollah Vali (McGill University),  
Alexei V. Smirnov (Yale University),  
and Joseph L. Kirschvink (California Institute of Technology)

Introduction

This auxiliary material contains the results of FMR, rock magnetic, electron diffraction, and energy dispersive spectroscopy (EDS) analyses of the Ancora core and also discusses the methods and implications of a paleogeographic re-interpretation of initial Eocene New Jersey. FMR parameters for samples from the core are presented in Table S1 ("2007pa001473-tableS1-sampledata.txt"). Remanent magnetization experiments are discussed in "2007pa001473-tex1-RemnantAndFORC.tex" and results presented in Table S1, Figure S1 ("2007pa001473-figS1-AncoraRmgProfiles.eps"), Figure S2 ("2007pa001473-figS2-AncoraCoercivity.eps"), and Figure S3 ("2007pa001473-figS3-AncoraARM.eps"). FORC analyses are described in "2007pa001473-tex1-RemnantAndFORC.tex", and a FORC distribution for one PETM clay sample is plotted in Figure S4 ("2007pa001473-figS4-Anc556-FORC.eps"). An electron diffraction pattern and an EDS spectrum for one PETM clay sample is presented in Figure S5 ("2007pa001473-figS5-Anc559-HRTEMandEDS.eps").

The paleogeographic analysis is discussed in "2007pa001473-tex2-Paleogeography.tex". Parameters used in the analysis are presented in Table S2 ("2007pa001473-tableS2-poleparameters.txt"). Paleolatitudes are presented in Table S3 ("2007pa001473-tableS3-paleolatitudes.txt").

1. 2007pa001473-tex1-RemnantAndFORC.tex describes the methods and results of remanent magnetization (alternating field, isothermal remanent magnetization, and anhysteretic remanent magnetization) and First Order Reversal Curve (FORC) analyses. The file is marked up in TeX.
2. 2007pa001473-tex2-Paleogeography.tex discusses our paleogeographic reconstruction of initial Eocene New Jersey, using the Faroe Islands flood basalt pole of Riisager et al. [2002]. The file is marked up in TeX.
3. 2007pa001473-tableS1-sampledata.txt Table S1. FMR and rock magnetic parameters for upper Paleocene to lower Eocene strata, ODP Leg 174AX, Ancora, New Jersey. FMR parameters are also presented in Figure 2, and rock magnetic parameters are also presented in Figure S1.
  - 3.1 Column "ft", feet, depth of sample.
  - 3.2 Column "depth", meters, depth of sample.
  - 3.3 Column "desc", description on sample, based on age, lithology, and FMR traits.
  - 3.4 Column "abs", arbitrary units, total FMR absorption
  - 3.5 Column "geff", effective g factor of absorption peak
  - 3.6 Column "A", FMR asymmetry ratio A
  - 3.7 Column "dBFWHM", mT, FMR full-width at half-maximum (in mT)
  - 3.8 Column "alpha", empirical FMR discriminant factor alpha
  - 3.9 Column "sIRM", Am<sup>2</sup>/kg, IRM determined after 350 mT pulse, "null" for samples not measured
  - 3.10 Column "Bcr", mT, coercivity of remanence, determined from the intersection of the IRM acquisition and demagnetization curves, "null" for samples not measured
  - 3.11 Column "chi\_ARMtoIRM", m/A, ratio of ARM susceptibility (assessed in 100 mT AF field and 0.1 mT DC biasing field) to IRM acquired in 100 mT field, "null" for samples not measured

4. 2007pa001473-tables2-poleparameters.txt Table S2. Parameters for applying Paleocene-Eocene Faroe Islands paleomagnetic pole to North America.
- 4.1 Column "using", description of site or pole
  - 4.2 Column "latitude", degrees, latitude
  - 4.3 Column "longitude", degrees, longitude
  - 4.4 Column "A95", degrees, A95 error angle
  - 4.5 Column "rotation\_angle", degrees, rotation angle
  - 4.6 Column "reference", source reference
5. 2007pa001473-tables3-paleolatitudes.txt Table S3. Ancora, New Jersey, paleolatitudes and facing directions for Faroe Islands volcanics and synthetic APWP poles
- 5.1 Column "reference\_pole", reference pole
  - 5.2 Column "pole\_lat", degrees, pole latitude
  - 5.3 Column "pole\_long", degrees, pole longitude
  - 5.4 Column "A95", degrees, A95 error angle, "null" where not determined
  - 5.5 Column "paleolat\_mean", degrees, mean estimated paleolatitude
  - 5.6 Column "paleolat\_confint\_lowerrange", degrees, lower range of confidence interval on estimated paleolatitude, "null" where A95 is not determined
  - 5.7 Column "paleolat\_confint\_upperange", degrees, upper range of confidence interval on estimated paleolatitude, "null" where A95 is not determined
  - 5.8 Column "facing", degrees, facing angle
  - 5.9 Column "reference", source reference
6. 2007pa001473-figS1-AncoraRmgProfiles.eps Figure S1. Fine quartz sand fraction,  $\delta^{13}\text{C}_{\text{inorganic}}$ , total FMR absorption, rock magnetic parameters, and IRM acquisition coercivity spectra for upper Paleocene to lower Eocene strata, ODP Leg 174AX, Ancora, New Jersey. Maximum IRM was imparted in a 350 mT field. Coercivity of remanence  $B_{cr}$  was determined from the intersection of IRM acquisition and demagnetization curves [Cisowski, 1981].  $\chi_{\text{ARM}}/\text{IRM}$  is the ratio of ARM susceptibility determined in a 100 mT alternating field and a 0.1 mT DC biasing field to IRM acquired in 100 mT field. Left edges of coercivity spectra align with drillcore depth.
7. 2007pa001473-figS2-AncoraCoercivity.eps Figure S2. Coercivity spectra from Ancora samples in late Paleocene silt, PETM clay, and early Eocene silt, determined from the derivative of IRM acquisition curves. Coercivity spectra for late Paleocene and early Eocene silt samples are exaggerated by a factor of 10.
8. 2007pa001473-figS3-AncoraARM.eps Figure S3. ARM acquisition curves for Ancora samples in late Paleocene silt, PETM clay, and early Eocene silt, determined in a 100 mT alternating field. The upper dotted line shows the reference curve of the magnetotactic bacterium *Magnetospirillum magneticum* AMB-1, while the lower dotted line shows the reference curve for highly interacting single domain magnetite in a chiton tooth.
9. 2007pa001473-figS4-Anc556-FORC.eps Figure S4. First-order reversal curve (FORC) distribution for an Ancora sample at 169.53 m. The distribution suggests the presence of stable single-domain magnetic particles (magnetofossils) with a unimodal grain-size distribution and weak between-chain or between-particle magnetic interactions. The color legend shows the distribution density. The smoothing factor  $SF = 2$ . The plot on the right shows a normalized vertical profile through the distribution maximum at 21.7 mT (dashed line). The mean half-width field  $H_{u/2} = 4.7$  mT.
10. 2007pa001473-figS5-Anc559-HRTEMandEDS.tif Figure S5. (a) Diffraction pattern and (b) energy dispersive spectroscopy (EDS) analysis of the particle shown in Figure 4d. (a) shows the spacing of 0.485 nm and 0.420 nm corresponding to the  $\{111\}$  and  $\{200\}$  planes of the magnetite, respectively. (b) demonstrates that the crystals are dominantly composed of iron and oxygen. Copper peaks result from the Cu TEM grid on which the sample was mounted. Traces of aluminium and silicon are likely from clay particles adsorbed onto the magnetite crystals.

## References

Besse, J., and V. Courtillot (2002), Apparent and true polar wander and the geometry of the geomagnetic field over the last 200 Myr, *J. Geophys. Res.*, 107, 2300, doi:2310.1029/2000JB000050.

Chen, A. P., R. Egli, and B. M. Moskowitz (in press), First-order Reversal Curve (FORC) diagrams of natural and cultured biogenic magnetic particles, *J. Geophys. Res.*, doi:10.1029/2006JB004575.

Cisowski, S. (1981), Interacting vs. non-interacting single-domain behavior in natural and synthetic samples, *Phys. Earth Planet. Int.*, 26, 56-62.

Diaz-Ricci, J. C., and J. L. Kirschvink (1992), Magnetic domain state and coercivity predictions for biogenic greigite (Fe<sub>3</sub>S<sub>4</sub>): a comparison of theory with magnetosome observations, *J. Geophys. Res.*, 97, 17309-17315.

Kopp, R. E., B. P. Weiss, A. C. Maloof, H. Vali, C. Z. Nash, and J. L. Kirschvink (2006), Chains, clumps, and strings: Magnetofossil taphonomy with ferromagnetic resonance spectroscopy, *Earth Planet. Sci. Lett.*, 247, 10-25.

Pan, Y., N. Petersen, M. Winklhofer, A. F. Davila, Q. Liu, T. Frederichs, M. Hanzlik, and R. Zhu (2005), Rock magnetic properties of uncultured magnetotactic bacteria, *Earth Planet. Sci. Lett.*, 237, 311-325.

Pike, C. R., A. P. Roberts, and K. L. Verosub (1999), Characterizing interactions in fine magnetic particle systems using first order reversal curves, *J. Appl. Phys.*, 85, 6660-6667.

Riisager, P., J. Riisager, N. Abrahamsen, and R. Waagstein (2002), New paleomagnetic pole and magnetostratigraphy of Faroe Islands flood volcanics, North Atlantic igneous province, *Earth Planet. Sci. Lett.*, 201, 261-276.

Srivastava, S. P., and W. R. Roest (1989), Seafloor spreading history II-IV, Atlantic Geoscience Centre, Geological Survey of Canada.

Storey, M., R. A. Duncan, and C. C. Swisher, III (2007), Paleocene-Eocene Thermal Maximum and the Opening of the Northeast Atlantic, *Science*, 316, 587-589.

Torsvik, T. H., J. Mosar, and E. A. Eide (2001a), Cretaceous-Tertiary geodynamics: a North Atlantic exercise, *Geophys. J. Int.*, 146, 850-866.

Torsvik, T. H., R. Van der Voo, J. G. Meert, J. Mosar, and H. J. Walderhaug (2001b), Reconstructions of the continents around the North Atlantic at about the 60th parallel, *Earth Planet. Sci. Lett.*, 187, 55-69.

Torsvik, T. H., R. Van der Voo, and T. F. Redfield (2002), Relative hotspot motions versus True Polar Wander, *Earth Planet. Sci. Lett.*, 202, 185-200.

Winklhofer, M., and G. T. Zimanyi (2006), Extracting the intrinsic switching field distribution in perpendicular media: A comparative approach, *J. Appl. Phys.*, 99, 08E710, doi:10.1063/1061.2176598.

## Remanent Magnetization Experiments

Remanent magnetization experiments were conducted using a 2G Enterprises SQUID magnetometer equipped with in-line alternating field (AF), anhysteretic remanent magnetization (ARM), and isothermal remanent magnetization (IRM) coils, as described in Kopp et al. [2006]. Parameters determined from these experiments are shown in Table S1 and Figure S1. Coercivity spectra determined from IRM acquisition experiments are shown in Figure S2, and ARM acquisition curves are shown in Figure S3.

Consistent with prior results from hysteresis experiments (Table S1), the IRM strength of samples from the PETM clay are 10-60 times higher than those of samples from underlying and overlying sediments (Figure S1). The coercivity of remanence of the PETM clay, which ranges from 53 to 69 mT, is lower than that of underlying and overlying samples (72-78 mT). Examination of the coercivity spectra (Figure S2) indicates that the increase in bulk coercivity is due to the influence of a high coercivity component, such as goethite or hematite. PETM clay also exhibits high values of anhysteretic susceptibility, consistent with those of magnetotactic bacteria (Figure S3).

## First Order Reversal Curve Analysis

First Order Reversal Curves (FORCs) were measured using a Princeton Measurements Alternating Gradient Magnetometer (MicroMag 2900) at Rutgers University. Measurement of a FORC begins by saturating the sample in a large positive magnetic field. Then the field is decreased to a reversal field  $H_a$ , and the FORC is defined by the set of induced magnetization measurements as the field is increased from  $H_a$  back to saturation. The FORC distribution is defined as a mixed derivative:  $\rho(H_a, H_b) \equiv -\partial^2 M(H_a, H_b) / \partial H_a \partial H_b$ , where  $M(H_a, H_b)$  is the magnetization at an applied field  $H_b$ , on the FORC with reversal point  $H_a$  ( $H_b \geq H_a$ ) [Pike, et al., 1999]. Quantitatively, the distribution  $\rho(H_a, H_b)$  at a point  $P$  is calculated by fitting a polynomial surface  $a_1 + a_2 H_a + a_3 H_a^2 + a_4 H_b + a_5 H_b^2 + a_6 H_a H_b$  on a local square grid centred at the point  $P$ . The value  $-a_6$  represents  $\rho(H_a, H_b)$  at  $P$ . A FORC diagram is a contour plot of  $\rho(H_a, H_b)$  with  $H_u = (H_b + H_a)/2$  and  $H'_c = (H_b - H_a)/2$  on the vertical and horizontal axes, respectively. The smoothing factor (SF) defines the number of points  $(2SF + 1)^2$  on the local grid.

The FORC distribution measured for an Ancora sample at 169.53 m (Figure S4) is elongate and roughly symmetric with respect to the  $H'_c$  axis. The distribution contours encircling a single maximum at  $H_{c,max} \approx 22$  mT are well separated from the diagram origin, suggesting stable single-domain particles (magnetofossils) with a unimodal grain-size distribution. The observed  $H'_{c,max}$  value is smaller than corresponding values observed for natural and cultured magnetosomes elsewhere [Chen, et al., in press; Pan, et al., 2005], consistent with a large mean size of magnetosomes in the Ancora PETM clay. The characteristic interaction field  $H_{u1/2} = 4.7$  mT (Figure S4, right) suggests weak between-chain or between-particle interaction [Pan, et al., 2005]. However, some widening of the outer contours for  $H'_c < 20$  mT hints at a stronger interaction, possibly due to minor magnetosome clumping in situ. The FORC data were processed using the “Forcobello” software, courtesy of Michael Winklhofer (Munich University) [Winklhofer and Zimanyi, 2006].

## Paleogeographic Reconstruction

The Faeroe Islands flood basalt pole of Riisager et al. [2002] considers minor dip of the flows and applies extensive alternating-field demagnetization, thermal demagnetization, and principal component analysis to at least 43 distinct flows, most of which are  $^{40}\text{Ar}$ - $^{39}\text{Ar}$  dated, directly and by correlation, between 56.0 and 55.1 Ma, effectively coincident with the PETM, best estimated at 55.6 Ma [Storey et al., 2007]. Other North Atlantic Igneous Province (NAIP) poles informing synthetic apparent polar wander paths (APWPs) used for conventional paleogeographic reconstruction [e.g., Besse and Courtillot, 2002; Torsvik, et al., 2001a; Torsvik, et al., 2001b; Torsvik, et al., 2002] were derived decades ago using blanket demagnetization, simpler statistical analysis, and more limited stratigraphic coverage, or they are subject to dating uncertainties. Riisager et al. [2002] attribute the  $\sim 10$  degrees steeper mean of those results to paleofield-undersampling or failure to remove present field contamination completely in the laboratory. Riisager et al. also note that expected-coeval NAIP poles are sometimes statistically distinct, attesting to some measure of ambiguity in the old results.

We rotate the new Faeroe Islands flood basalts pole from the Rockall Plateau microplate to North America using the “56.0” Ma Euler pole specified by Royer et al. [1992], citing Srivastava and Roest [1989] (Table S2; application of conventional,  $\sim 55$  Ma synthetic APWP poles in Table S3). Applying the “55.0” Ma Eurasian Euler pole with same source would yield a shallower paleolatitude for New Jersey by  $\sim 1$  degree, and a less westward facing direction by a similar amount. While Torsvik et al. [2001a] note that conventional continent reconstructions across the North Atlantic neglect tectonism prior to successful Atlantic rifting, rotation prescribed by marine magnetic anomalies and fracture zones are preferred at ages younger than or equal to  $\sim 55$  Ma.

To offer a measure of uncertainty in each calculated paleolatitude, we assign  $A_{95}$  for each reference pole as  $\alpha_{95}$  at Ancora’s location for the prescribed declination and inclination. This is not robust but in this case it is conservative, overestimating paleolatitude uncertainty slightly. Robust uncertainty analysis would require distribution analysis of site-level paleomagnetic data yielding the constituent reference poles, which is beyond the scope of this paper. In any case, uncertainty in Euler pole location for rotating the most robust, Faeroe Islands paleomagnetic pole onto North America is probably of similar magnitude to the paleolatitude uncertainty overestimate introduced by applying  $A_{95}$  as  $\alpha_{95}$ .

We follow Besse and Courtillot [2002] and many other authors in noting that temporal and spatial coverage in the global paleomagnetic database is generally insufficient to demonstrate or to deny short and/or fast bursts of true polar wander (TPW). It is possible that such TPW accounts for the apparent  $\sim 10$  degrees anomalous paleolatitude indicated by application of the new Faeroe Islands pole relative to the expected paleolatitude based on synthetic APWPs and old (here considered superseded) NAIP poles. Full consideration of this possibility and description of a global paleogeography determined by application of Riisager et al. [2002]’s Faeroe Islands pole are beyond the scope of this paper.

| ft     | depth  | desc                             | abs | geff  | A    | dBFWHM | alpha | sIRM     | Bcr  | chi_ARMtoIRM |
|--------|--------|----------------------------------|-----|-------|------|--------|-------|----------|------|--------------|
| 539.14 | 164.33 | Eocene silt                      | 47  | 2.062 | 0.9  | 250    | 0.4   | NULL     | NULL | NULL         |
| 541.98 | 165.2  | Eocene silt                      | 39  | 2.059 | 0.89 | 255    | 0.4   | 8.20E-05 | 77.5 | 8.00E-04     |
| 542.7  | 165.41 | Eocene silt                      | 44  | 2.065 | 0.91 | 248    | 0.4   | NULL     | NULL | NULL         |
| 543.14 | 165.55 | late PETM transitional clay      | 64  | 1.97  | 0.69 | 193    | 0.31  | 3.05E-03 | 65.3 | 2.80E-03     |
| 543.99 | 165.81 | late PETM transitional sand lens | 97  | 2.03  | 0.73 | 212    | 0.33  | NULL     | NULL | NULL         |
| 543.99 | 165.81 | late PETM transitional clay      | 101 | 2.03  | 0.72 | 215    | 0.33  | NULL     | NULL | NULL         |
| 544.87 | 166.08 | late PETM transitional clay      | 123 | 2     | 0.68 | 201    | 0.31  | 3.09E-03 | 68.7 | 2.70E-03     |
| 550.2  | 167.7  | PETM clay                        | 189 | 1.993 | 0.69 | 178    | 0.29  | NULL     | NULL | NULL         |
| 551.73 | 168.17 | PETM clay                        | 212 | 2     | 0.7  | 183    | 0.3   | 4.65E-03 | 54.9 | 2.70E-03     |
| 551.93 | 168.23 | PETM clay                        | 74  | 1.993 | 0.7  | 170    | 0.28  | NULL     | NULL | NULL         |
| 552.94 | 168.54 | PETM clay                        | 205 | 2.02  | 0.71 | 182    | 0.3   | NULL     | NULL | NULL         |
| 553.84 | 168.81 | PETM clay                        | 156 | 2.012 | 0.69 | 185    | 0.3   | 4.66E-03 | 61.4 | 2.70E-03     |
| 553.87 | 168.82 | PETM clay                        | 171 | 2.01  | 0.7  | 190    | 0.3   | NULL     | NULL | NULL         |
| 554.83 | 169.11 | PETM clay                        | 206 | 1.997 | 0.69 | 182    | 0.3   | 3.83E-03 | 53   | 2.70E-03     |
| 556.19 | 169.53 | PETM clay                        | 167 | 2.027 | 0.74 | 179    | 0.3   | NULL     | NULL | NULL         |
| 557.39 | 169.89 | PETM clay                        | 124 | 1.993 | 0.67 | 179    | 0.29  | NULL     | NULL | NULL         |
| 557.85 | 170.03 | PETM clay                        | 196 | 2.031 | 0.75 | 170    | 0.29  | NULL     | NULL | NULL         |
| 558.1  | 170.11 | PETM clay                        | 182 | 2.004 | 0.71 | 181    | 0.3   | NULL     | NULL | NULL         |
| 559.1  | 170.41 | PETM clay                        | 195 | 2.014 | 0.7  | 176    | 0.29  | NULL     | NULL | NULL         |
| 559.59 | 170.56 | PETM clay                        | 176 | 2     | 0.68 | 181    | 0.29  | NULL     | NULL | NULL         |
| 560.32 | 170.79 | PETM clay                        | 141 | 2.004 | 0.69 | 188    | 0.3   | NULL     | NULL | NULL         |
| 560.72 | 170.91 | PETM clay                        | 162 | 2.017 | 0.74 | 164    | 0.29  | 1.74E-03 | 64.4 | 3.20E-03     |
| 561.22 | 171.06 | early PETM transitional clay     | 142 | 2.024 | 0.73 | 205    | 0.33  | 2.71E-03 | 62.2 | 2.10E-03     |
| 561.73 | 171.22 | early PETM transitional clay     | 135 | 2.044 | 0.75 | 215    | 0.34  | NULL     | NULL | NULL         |
| 561.83 | 171.25 | early PETM transitional clay     | 147 | 2.031 | 0.75 | 210    | 0.33  | NULL     | NULL | NULL         |
| 562.22 | 171.36 | Paleocene silt                   | 128 | 2.062 | 0.92 | 233    | 0.38  | NULL     | NULL | NULL         |
| 562.75 | 171.53 | Paleocene silt                   | 102 | 2.12  | 1.06 | 237    | 0.41  | NULL     | NULL | NULL         |
| 563.07 | 171.62 | Paleocene silt                   | 112 | 2.071 | 0.99 | 232    | 0.4   | NULL     | NULL | NULL         |
| 563.88 | 171.87 | Paleocene silt                   | 88  | 2.055 | 0.95 | 234    | 0.39  | NULL     | NULL | NULL         |
| 564.15 | 171.95 | Paleocene silt                   | 105 | 2.055 | 0.95 | 238    | 0.4   | NULL     | NULL | NULL         |
| 565.03 | 172.22 | Paleocene silt                   | 94  | 2.084 | 0.98 | 223    | 0.39  | NULL     | NULL | NULL         |
| 565.83 | 172.46 | Paleocene silt                   | 110 | 2.084 | 1.04 | 235    | 0.41  | 1.37E-04 | 72.3 | 6.00E-04     |

**using****latitude longitude A95 rotation\_angle reference**

|   |       |        |      |      |        |  |
|---|-------|--------|------|------|--------|--|
| Site: Ancora, New Jersey                                      | 39.7  | 285.2  | null | null |        | null   |
| Paleomagnetic Pole: Faeroe PE flood basalts on Rockall microp | 71.4  | 154.7  | 6    | null |        | Riisager et al. (2002)                         |
| Euler Pole: Rockall to North America "56.0" Ma                | 54.86 | 143.39 | null |      | -11.99 | Royer et al. (1992) citing Srivastava and Roes |

| reference_pole  | pole_lat | pole_long | A95  | paleolat_mean | paleolat_confint_lowerrange | paleolat_confint_upperrange | facing | reference                         |
|---|----------|-----------|------|---------------|-----------------------------|-----------------------------|--------|-----------------------------------|
| Faeroe PE basalts rotated onto North America              | 69.56    | 163.75    | 6    | 27.3          |                             | -4.6                        | 5.2    | -19.6 Riisager et al. (2002)      |
| North America APWP, 10 My window @ 55 Ma                  | 77.9     | 183.4     | 4.2  | 36.3          |                             | -4.1                        | 4.5    | -14.7 Besse and Courtillot (2002) |
| North America APWP @ 55 Ma                                | 77.1     | 174.9     | 2.6  | 34.3          |                             | -1.5                        | 2.5    | -14.7 Torsvik et al. (2002)       |
| North America APWP @ 55 Ma, paleomagnetic pole-referenced | 77.1     | 172.9     | 2.5  | 33.9          |                             | -2.4                        | 2.5    | -14.4 Torsvik et al. (2001a)      |
| North America APWP @ 55 Ma, hotspot-referenced            | 83.6     | 143.9     | 2.5  | 34.6          |                             | -2.4                        | 2.5    | -4.9 Torsvik et al. (2001a)       |
| North America APWP, 20 My window @ 55 Ma                  | 79.86    | 164.56    | 3.76 | 34            |                             | -3.9                        | 3.9    | -10.5 Torsvik et al. (2001b)      |
| North America-Eurasia splined APWP, 20 My window @ 55 Ma  | 75.39    | 174.43    | null | 33.3          | null                        |                             |        | -16.4 Torsvik et al. (2001b)      |

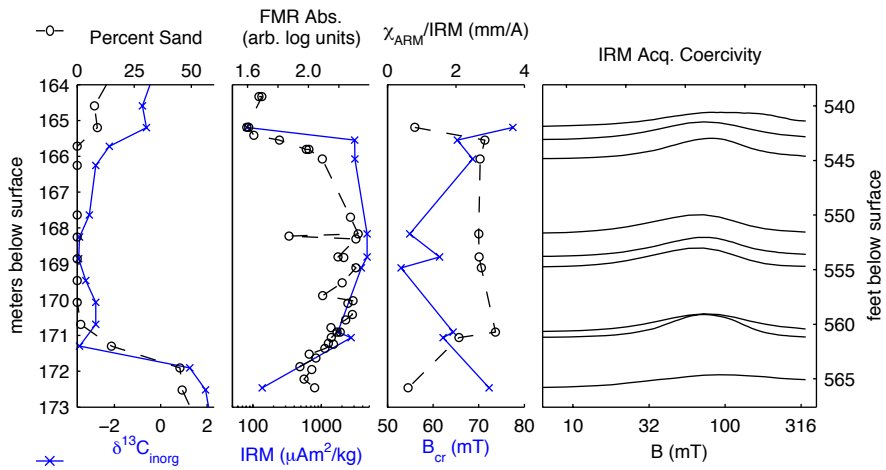


Figure S1: Fine quartz sand fraction,  $\delta^{13}C_{inorganic}$ , total FMR absorption, rock magnetic parameters, and IRM acquisition coercivity spectra for upper Paleocene to lower Eocene strata, ODP Leg 174AX, Ancora, New Jersey. Maximum IRM was imparted in a 350 mT field. Coercivity of remanence  $B_{cr}$  was determined from the intersection of IRM acquisition and demagnetization curves (Cisowski, 1981).  $\chi_{ARM}/IRM$  is the ratio of ARM susceptibility determined in a 100 mT alternating field and a 0.1 mT DC biasing field to IRM acquired in 100 mT field. Left edges of coercivity spectra align with drillcore depth.

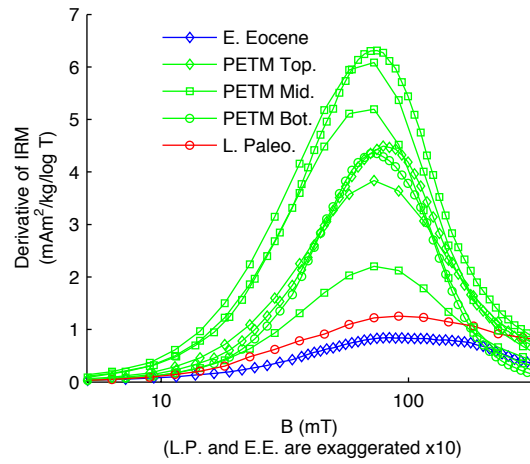


Figure S2: Coercivity spectra from Ancora samples in late Paleocene silt, PETM clay, and early Eocene silt, determined from the derivative of IRM acquisition curves. Coercivity spectra for late Paleocene and early Eocene silt samples are exaggerated by a factor of 10.

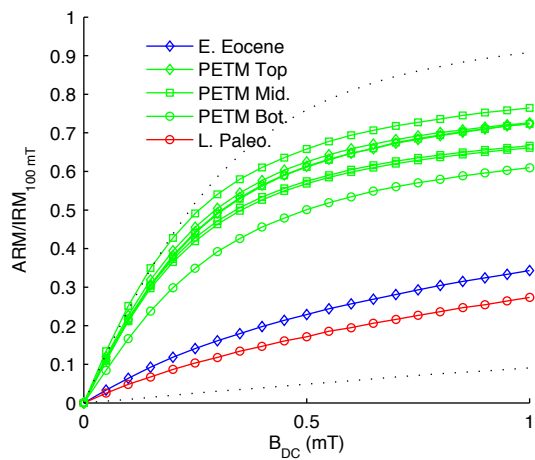


Figure S3: ARM acquisition curves for Ancora samples in late Paleocene silt, PETM clay, and early Eocene silt, determined in a 100 mT alternating field. The upper dotted line shows the reference curve of the magnetotactic bacterium *Magnetospirillum magneticum* AMB-1, while the lower dotted line shows the reference curve for highly interacting single domain magnetite in a chiton tooth.

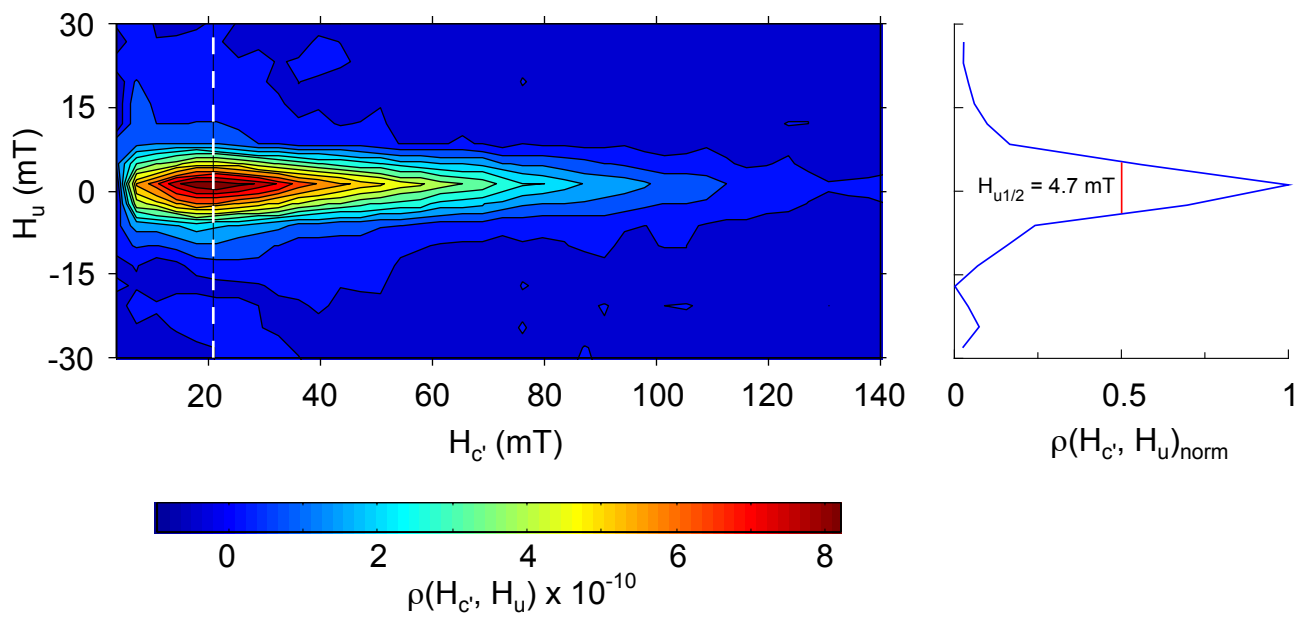


Figure S4: First-order reversal curve (FORC) distribution for an Ancora sample at 169.53 m. The distribution suggests the presence of stable single-domain magnetic particles (magnetofossils) with a unimodal grain-size distribution and weak between-chain or between-particle magnetic interactions. The color legend shows the distribution density. The smoothing factor  $SF = 2$ . The plot on the right shows a normalized vertical profile through the distribution maximum at 21.7 mT (dashed line). The mean half-width field  $H_{u1/2} = 4.7$  mT.

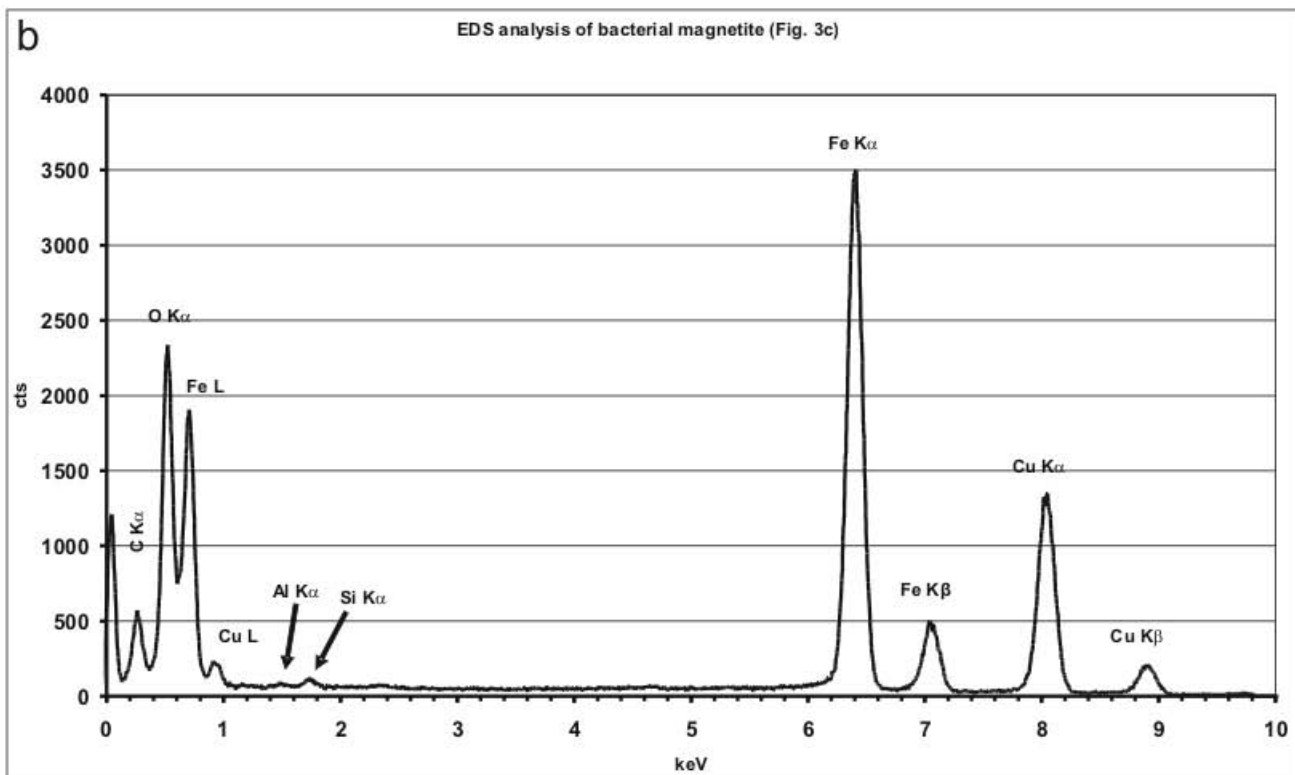
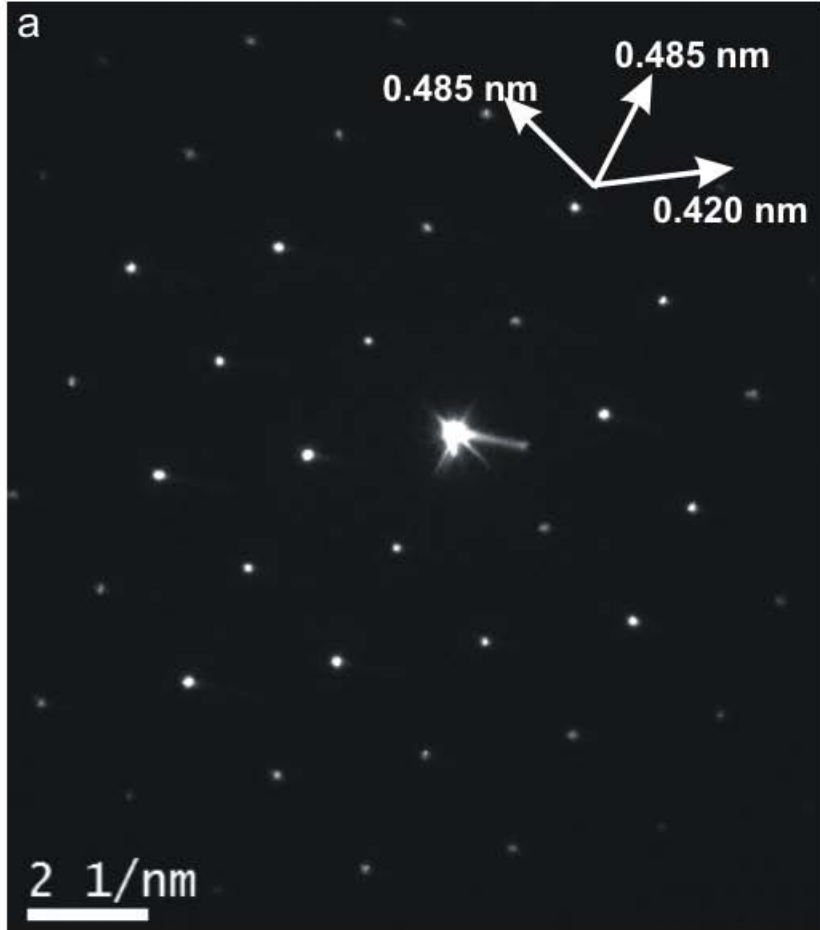


Figure S5: (a) Diffraction pattern and (b) energy dispersive spectroscopy (EDS) analysis of the particle shown in Figure 4d. (a) shows the spacing of 0.485 nm and 0.420 nm corresponding to the {111} and {200} planes of the magnetite, respectively. (b) demonstrates that the crystals are dominantly composed of iron and oxygen. Copper peaks result from the Cu TEM grid on which the sample was mounted. Traces of aluminium and silicon are likely from clay particles adsorbed onto the magnetite crystals.